Differential Modulation of Cardiac Ca^{2+} Channel Gating by β-Subunits

Igor Dzhura* and Alan Neely*†
*Department of Physiology, Texas Tech University, Lubbock, Texas USA; and †Centro de Neurosciencias de Valparaíso, University of Valparaíso, Valparaíso, Chile

ABSTRACT To investigate the mechanisms that increase ionic currents when Ca^{2+} channels' α_1 subunits are co-expressed with the β-subunits, we compared channel activity of $Ca_V1.2$ (α_{1C}) co-expressed with β_{1a} and β_{2a} in *Xenopus* oocytes. Normalized by charge movement, ionic currents were near threefold larger with β_{2a} than with β_{1a}. At the single-channel level, the open probability (P_o) was over threefold larger with β_{2a}, and traces with high P_o were more frequent. Among traces with $P_o >$ 0.1, the mean duration of burst of openings (MBD) were nearly twice as long for $\alpha_{1C}\beta_{2a}$ (15.1 ± 0.7 ms) than for $\alpha_{1C}\beta_{1a}$ (8.4 ± 0.5 ms). Contribution of endogenous β_{3xo} was ruled out by comparing MBDs with α_{1C}-cRNA alone (4.7 ± 0.1 ms) with β_{3xo} (14.3 ± 1.1 ms), and with β_{1b} (8.2 ± 0.5 ms). Open-channel current amplitude distributions were indistinguishable for $\alpha_{1C}\beta_{1a}$ and $\alpha_{1C}\beta_{2a}$, indicating that opening and closing kinetics are similar with both subunits. Simulations with constant opening and closing rates reproduced the microscopic kinetics accurately, and therefore we conclude that the conformational change-limiting MBD is differentially regulated by the β-subunits and contributes to the larger ionic currents associated with β_{2a}, whereas closing and opening rates do not change, which should reflect the activity of a separate gate.

INTRODUCTION

High-voltage Ca^{2+} channels are multisubunit membrane proteins composed of four nonhomologous subunits: the α_1 subunit, encompassing all the structural elements of a functional voltage-activated channel; and three regulatory subunits: α_2/δ, β, and γ. Co-expression of α_2/δ- and/or β-subunits with the α_1 subunit increases macroscopic currents, suggesting that these subunits may regulate channel abundance (Wei et al., 1991; Williams et al., 1992). However, increased ionic currents often displayed significant alteration in time and voltage dependence (Stea et al., 1993; Singer et al., 1991), indicating that the function of the channel may also be modulated by the regulatory subunit. Through gating current measurements we showed that co-expression of β_{2a} augments ionic conductance fivefold without changing the maximum gating charge movement (Neely et al., 1993). The coupling efficiency of charge movement to pore opening is also increased by the β-subunit in a neuronal Ca^{2+} channel ($Ca_V2.3$) expressed in *Xenopus* oocytes (Olcese et al., 1996).

Further insight in the functional changes associated with co-expression of the β-subunit was gained by comparing single-channel activity of $Ca_V1.2$ expressed with or without β_{2a} (Wakamori et al., 1993; Neely et al., 1995; Costantin et al., 1998). All these studies rule out changes in single-channel conductance and report increases in the frequency of long openings to explain, at least partially, how ionic currents may be increased by the β-subunit. Since native Ca^{2+} channels activate in different gating modes with characteristic open probability (P_o) (Cavalie et al., 1986; Hess et al., 1984), the frequency of long openings may be increased by β if the interaction with α_1 promotes modes of higher P_o. Shift in gating modes with different subunit combinations has been shown to occur in the acetylcholine-activated channel (Naranjo and Brehm, 1993). However, rather than an increase in the fraction of time spent in the high P_o mode, co-expression of β_{2a} with α_{1C} was correlated instead with an increase in the frequency of mode switching (Costantin et al., 1998). Co-expression of the neuronal isoform of β with $Ca_V2.1$ led to an increase in the mean open-time also, with no evidence of mode shifting (Wakamori et al., 1999).

A common assumption in these co-expression experiments was that contribution of endogenous subunits is negligible. Today this view is no longer tenable since we know that β releases α_1 from the endoplasmic reticulum (Bichet et al., 2000) and is required for the expression (Tareilus et al., 1997) and proper targeting of channels (Chien et al., 1995; Brice et al., 1997). This combined effect on expression and function was suggested to reflect the binding of multiple β-subunits: association with one β would be required for expression whereas functional changes would come about with additional β-subunits. In this scheme, lower coupling efficiencies may arise from channels with an incomplete complement of β, as it would be the case if, for example, β_{1a} expresses less efficiently than β_{2a} (Birnbaumer et al., 1998). Here we compare the gating behavior of channels from oocytes co-expressing α_{1C} with two different β-subunits: the cardiac (β_{2a}) and the skeletal (β_{1a}) muscle isoform. We show that oocytes expressing $\alpha_{1C}\beta_{2a}$ display higher ionic-to-gating current ratio than the ones expressing $\alpha_{1C}\beta_{1a}$. At the single-channel level, we found that the P_o for channels from $\alpha_{1C}\beta_{2a}$ expressing oocytes is severalfold higher than for $\alpha_{1C}\beta_{1a}$, with an

Submitted January 22, 2003, and accepted for publication March 17, 2003.

Address reprint requests to Alan Neely, Centro de Neurociencias de Valparaíso, Universidad de Valparaíso, Gran Bretaña 1111, Valparaíso, Chile. Tel.: 56-32-50-8054; Fax: 56-32-28-3320; E-mail: alan.neely@uv.cl.
Igor Dzhura's current address is Dept. of Medicine, Division of Cardiology, Vanderbilt University Medical Ctr., 315 MRB II, 2220 Pierce Ave., Nashville, TN 37232.

0006-3495/03/07/274/16 $2.00

increase in the number of sweeps with higher P_o. Among traces with $P_o > 0.1$, MBD was nearly twice as long for $\alpha_{1C}\beta_{2a}$ than for $\alpha_{1C}\beta_{1a}$, suggesting that the β-subunit modulates gating within a mode. We also analyzed oocytes expressing other subunit combinations to rule out channel heterogeneity as the source of this functional difference.

The duration of burst of openings is determined by the transition rate to long-lived closed state and the ratio between opening and closing rates (Colquhoun and Sakmann, 1985). When opening and closing events are well-resolved, all these rates can be obtained directly from dwell-time histograms. In the presence of the dihydropyridine agonist Bay K 6844, as used here, most openings appear well-resolved, but they are often interrupted by brief closures that, when missed, lead to an overestimation of the open state's lifetime. This error cannot be corrected for in a model-independent manner (McManus and Magleby, 1991). To test for differences in opening and closing rates in a detection-independent manner, we compared the distribution of current amplitudes of $\alpha_{1C}\beta_{2a}$ and $\alpha_{1C}\beta_{1a}$ and found no difference. Opening and closing rates derived directly from these distributions (Marks and Jones, 1992; Prodhom et al., 1989) were over 10-fold faster than predicted from dwell-time histograms. Simulated single-channel activity with these faster rates reproduced open-time and burst-duration histograms for both subunit combinations when only the rate leading to long-lived closed states was changed. Changes in fast gating that increase MBD visibly alter the open-channel amplitude distribution, indicating that a conformational change leading to long-lived closed state is being differentially regulated by the β-subunits and that modulation of this transition partially accounts for the increases in coupling efficiencies. In contrast, closing and opening rates do not appear to sense the presence of the β-subunit, indicating that a separate gating mechanism is involved.

METHODS

RNA synthesis and oocytes preparation

The cardiac Ca^{2+} channel α_1 subunit was an amino terminal deletion mutant of the rabbit $Ca_V1.2$ (ΔN60) that yields larger ionic and gating currents without changes in kinetics or sensitivity to the modulation by the β-subunit (Wei et al., 1996). The β_{2a} (Wei et al., 1991) and β_{1b} (Pragnell et al., 1991) subunits were from rat, the β_{1a} was from rabbit (Ruth et al., 1989) and β_{3xo} is a β_3-like subunit cloned from *Xenopus* oocytes (Tareilus et al., 1997). ΔN60, β_{2a}, and β_{3xo} subunits were subcloned into pAGA2 (Sanford et al., 1991), β_{1a} in pGEM-3, and β_{1b} in pBS. pAGAΔN60, pAGAβ_{2a} and pAGAβ_{3xo} cDNA were linearized with *Hin*dIII; pBSβ_{1b} with *Not*I and pGEMβ_{1a} with *Xba*I (New England Biolabs, Beverly, MA). RNAs were synthesized in vitro with the mMESSAGE MACHINE (Ambion, Austin, TX) according to the manufacturer instructions and resuspended in 10 μl of water at 4–6 μg/μl. Stock solutions were diluted from 10- to 100-fold and the dilutions yielding larger expression and maximal functional changes were chosen for subsequent experiments. For the oocytes included in the article, cRNA were diluted as follows: β_{2a} 1:40, β_{1a} 1:20, β_{1b} 1:20, β_{3xo} 1:60, and ΔN60 1:20. 50 nl of cRNA were injected per oocyte using a 10-μl automatic injector (Drummond Scientific, Broomall, PA).

Large *Xenopus* female frogs (Nasco, Modesto, CA) were anaesthetized by immersion in 0.15% tricaine for 15 min. One or two lobes of an ovary were removed through a 10- to 12-mm abdominal incision under sterile conditions. Oocytes were harvested from the same frog up to five times, allowing at least six weeks of recovery. This procedure, general care, and handling of *Xenopus* frogs were carried out according to a protocol approved by the Institutional Animal Care Committee of Texas Tech University Health Sciences Center. Oocytes were defolliculated by collagenase treatment (2 mg/ml, type II from Worthington Biochemical, Lakewood, NJ) for 30 min in Ca^{2+}-free solution (82.5 mM NaCl, 2.5 mM KCl, 1 mM $MgCl_2$, and 5 mM HEPES titrated to pH 7.6 with NaOH). Collagenase treatment was stopped by repeated rinses with Ca^{2+}-free media that was then replaced by SOS (100 mM NaCl, 2 mM KCl, 1.8 mM $CaCl_2$, 1 mM $MgCl_2$, and 5 mM HEPES titrated to pH 7.6 with NaOH) in several partial dilution steps over a period of 1 h. Oocytes were maintained at 19.5°C in SOS supplemented with Na-pyruvate (2.5 mM), gentamycin (50 or 200 μg/ml), and Verapamil (10 μM). The latter appears to increase survival of oocytes expressing large Ca^{2+} currents, although a systematic survey was not carried out.

Recording techniques

Macroscopic currents were recorded using the cut-open oocyte voltage-clamp technique (Taglialatela et al., 1992) with a CA-1 amplifier (Dagan, Minneapolis, MN). Oocyte membrane exposed to the bottom chamber was permeabilized by a brief treatment with 0.1% saponin. The voltage pipettes were filled with 2 M tetramethylammonium-methanesulfonate, 50 mM NaCl, and 10 mM EGTA and had tip resistance from 600–1200 kΩ. Data acquisition and analysis were performed using the pCLAMP6 system (Axon Instruments, Foster City, CA). The external solution contained 10 mM Ba^{2+}, 96 mM *n*-methylglucamine, and 10 mM HEPES, and the pH was adjusted to 7.0 with methanesulfonic acid (MES). The internal solution contained 120 mM *n*-methylglucamine, 10 mM EGTA, and 10 mM HEPES and the pH was adjusted to 7.0 with MES.

Patch-clamp recordings of single channels were performed with an Axopatch-200A with an integrating headstage (Axon Instruments, Foster City, CA). Patch pipettes were pulled from aluminum silicate capillary (Sutter Instrument, Novato, CA) and filled with a solution containing 76 mM Ba^{2+}, 10 mM HEPES, and 100 nM S(−)Bay K 8644 (Research Biochemical International, Natick, MA). The pH was adjusted to 7.0 with MES. Pipette resistance ranged from 4 to 7 MΩ. Vitelline membranes were removed manually after exposure to a hyperosmotic solution (2–5 min) containing 200 mM K-glutamate, 20 mM KCl, 1 mM $MgCl_2$, 10 mM EGTA, 10 mM HEPES, and 100 nM S(−) Bay K 8644 and titrated to pH 7.2 with KOH. Oocytes were then placed in the recording chamber with a depolarizing solution of the following composition: 110 mM K^+, 10 mM HEPES titrated to pH 7.0 with MES. Channels were activated by 185-ms pulses to 0 mV at 1 Hz from a holding potential of −70 mV sampled at 20 kHz and filtered at 2 kHz.

Unless noted otherwise, all chemical and reagents were from Sigma-Aldrich (St. Louis, MO).

Data analysis

Dwell-time histograms

Dwell-time histograms were constructed with the dedicated software TRANSIT (Van Dongen, 1996) from traces corrected for capacitive transients and leakage currents by subtracting the average of traces without openings. This software also yields a P_o estimate by calculating the fraction of time spent in the open state. The number of samples was reduced by one-half before the analysis resulting in an effective sampling rate of 10 kHz. Multiexponential probability density functions (PDF) were adjusted to fit dwell-time histograms displayed in Sigworth-Sine coordinates using a maximum likelihood algorithm (Sigworth and Sine, 1987). The first bin included for the analysis of closed and open-time histograms was from 0.36 to 0.44 ms that corresponds to the first bin followed by a nonempty bin. This eliminates events shorter than three times the dead time of the system (≈0.1 ms).

A burst was defined as a series of consecutive openings separated by closures briefer than τ_{crit}, such that

$$1 - \exp(-\tau_{crit}/\tau_S) = \exp(-\tau_{crit}/\tau_L). \quad (1)$$

Here, τ_L and τ_S correspond to the mean duration of long and short closures respectively obtained from fitting closed-duration histograms with a double-exponential PDF. Shut intervals pertaining to either long- or short-lived closed states will have the same probability of being misclassified if their duration is equal to τ_{crit} (Colquhoun and Sakmann, 1985).

All-points histograms

Opening and closing rate constants were extracted from all-point histograms according to a method introduced by Fitzhugh (1983) and Yellen (1984) and later adapted for Ca^{2+} channels by Marks and Jones (1992). Briefly, the filtered flicker of a channel between a single open and closed state is described by a β-distribution in the absence of noise,

$$B(x) = x^{(\alpha^*-1)} \times (1-x)^{(\beta^*-1)}, \quad (2)$$

where $\alpha^* = \tau\, k_O$ and $\beta^* = \tau\, k_C$, k_O and k_C are the opening and closing rates, respectively, τ is the time constant of the filters, and x is the normalized current amplitude (*open* = 1 and *closed* = 0). The value of τ was calculated as in Marks and Jones (1992). Background noise was included as a convolution of $B(x)$ with a Normal distribution describing baseline fluctuations (Villarroel et al., 1988),

$$A(x) = B(x) * A\, e^{[-0.5((x-\mu)/\sigma)^2]}, \quad (3)$$

where μ and σ are the mean and standard deviation of the baseline noise, respectively.

To eliminate capacitive transients, a multiexponential function that best described the transient at the beginning of the test pulse was subtracted from each pulse. After this subtraction, the beginning and end of the traces were forced to '0' eliminating any remaining capacitive component. The data was then filtered digitally at 300 Hz with a Gaussian filter. Traces whose baseline deviated from zero were readjusted by eye. All-point histograms were then constructed with FETCHAN6 (Axon Instrument) and exported to an Excel (Microsoft, Seattle, WA) spreadsheet for further analysis. Bins between −0.3 and +0.3 pA were normalized to a total area of '1' and a Normal distribution adjusted. The theoretical Normal distribution was then convolved to $B(x)$ to obtain $A(x)$, which was then compared to the open-channel amplitude PDF (APDF). The convolution was performed with a program originally written in QuickBasic by Marks and Jones (1992), later adapted as an Excel macro. Amplitude bins of all-points histograms were divided by the single-channel current amplitude and the area normalized by the total count between 70% and 150% of the amplitude to generate the APDF. Single-channel current amplitudes were first measured in prolonged openings and then adjusted (±5%) to improve the quality of the fit of the APDF.

Simulation of single-channel activity

The program CSIM 2.0 (Axon Instruments) was used to simulate single-channel activity. The single-channel conductance was set to 17 pS and the reversal potential to +70 mV. Sampling rate was set at 10 kHz, the filter at 1.7 kHz, and 0.18 pA of noise was added. The cutoff frequency was determined by measuring the rise time (10–90% in 200 μs) of single-channel openings from the experimental records.

RESULTS

Macroscopic currents

Fig. 1 compares voltage-clamp traces and current-voltage plots from oocytes expressing either $\alpha_{1c}\beta_{2a}$ or $\alpha_{1c}\beta_{1a}$. To separate differences in function and expression for each oocyte, we normalized inward currents measured at the end of each pulse by the amount of charge movement measured at the onset of a depolarizing step (Q_{on}) to the current reversal potential (+55 to +67 mV, Fig. 1 *B*). At these voltages, contribution of ionic current is negligible (Fig. 1 *B*) and charge movement is expected to have reached their maximum for the different subunit combinations of Ca^{+2} channels expressed in oocytes (Neely et al., 1993). Channel expression, as assayed by Q_{on}, was highly variable and not significantly different for the two subunit combinations. In 10 mM Ba^{2+} the average Q_{on} was 503 ± 129 *n*C ($n = 8$) and 283 ± 117 *n*C ($n = 7$) for $\alpha_{1c}\beta_{1a}$ and $\alpha_{1c}\beta_{2a}$ respectively. On the other hand, when ionic currents were normalized by Q_{on}, we observed that α_{1C} combined with β_{2a} yields larger ionic currents (−2.61 ± 0.62 *n*A/*p*C at +10 mV, with $n = 7$) than when combined with β_{1a} (−0.97 ± 0.26 *n*A/*p*C at +20 mV, with $n = 8$). Such an increase in coupling efficiency between charge movement and ionic current can occur through an increase in the single-channel conductance and/or the P_o of the channel. Since these issues are addressed through single-channel recordings taken in the presence of channel agonist

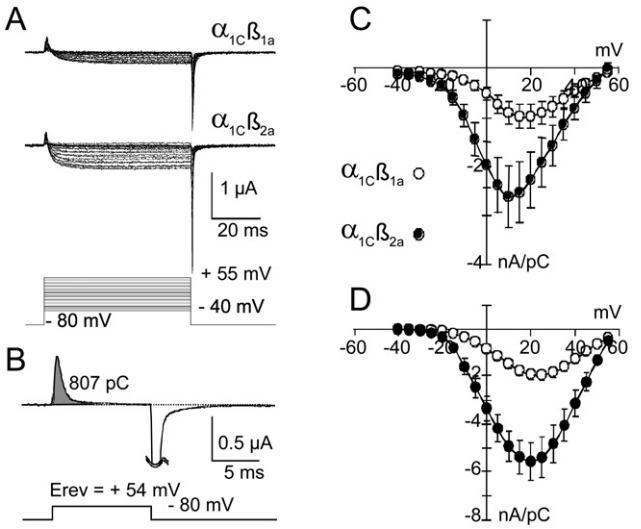

FIGURE 1 Current-voltage relationship normalized by charge movement for oocytes expressing $\alpha_{1C}\beta_{1a}$ or $\alpha_{1C}\beta_{2a}$. (*A*) Superimposed voltage-clamp traces during 60-ms depolarizing steps from −40 mV to +55 mV in 5-mV increments from two oocytes; one expressing $\alpha_{1C}\beta_{1a}$ (*top*) and the other $\alpha_{1C}\beta_{2a}$ (*bottom*) in 10 mM external Ba^{+2}. Membranes were held at −80 mV between depolarizing pulses and linear components were subtracted by the $p/-4$ protocol from the same holding voltage. Currents were sampled at 5 kHz and filtered at 1 kHz. (*B*) Example of charge-movement measurement (*shaded area*) at the onset of a depolarization to the current reversal potential from an oocyte expressing $\alpha_{1C}\beta_{2a}$. (*C*) Average IV plots normalized by charge-movement from eight oocytes expressing $\alpha_{1C}\beta_{1a}$ (○) and seven oocytes expressing $\alpha_{1C}\beta_{2a}$ (●). Error bars represent SE. (*D*) Normalized IV plots in the presence of 0.1 μM (−)Bay K 8644 and 76 mM external Ba^{2+} from eight oocytes expressing $\alpha_{1C}\beta_{1a}$ (○) and seven oocytes expressing $\alpha_{1C}\beta_{2a}$ (●).

and high external Ba^{2+} to overcome bandwidth and noise limitations, we also compared normalized ionic currents in 0.1 μM S(−) Bay K 8644 and 76 mM external Ba^{2+}. In these recording conditions, $\alpha_{1c}\beta_{2a}$ expressing oocytes yield −5.56 *n*A/*p*C (at +20 mV, with $n = 7$) compared to −1.92 *n*A/*p*C (at +25 mV, with $n = 8$) for $\alpha_{1c}\beta_{1a}$. (Fig. 1 *D*) and Q_{on} was 205 ± 21 *n*C ($n = 8$) for $\alpha_{1c}\beta_{1a}$ and 250 ± 92 *n*C ($n = 7$) for $\alpha_{1c}\beta_{2a}$.

Single-channel activity

Single-channel currents were measured at −30, 0, and +30 mV from oocytes expressing each subunit combination and compiled to calculate single-channel conductances. As predicted from previous work comparing α_{1C} and $\alpha_{1C}\beta_{2a}$ (Wakamori et al., 1993), the single-channel conductance of $\alpha_{1C}\beta_{1a}$ and $\alpha_{1C}\beta_{2a}$ is the same (17.2 ± 0.8 pS and 17.6 ± 0.6 pS for $\alpha_{1C}\beta_{1a}$ or $\alpha_{1C}\beta_{2a}$, respectively) and thus, we focused our analysis in differences in P_o at 0 mV. At this potential, differences in the amplitude in macroscopic currents were large (fourfold) and bursts of openings are well-separated by long closures. To evaluate the changes in P_o, we selected seven and four patches from oocytes expressing $\alpha_{1C}\beta_{1a}$ and $\alpha_{1C}\beta_{2a}$, respectively, that lacked simultaneous openings and displayed comparable activity at the beginning and end of the recordings (Fig. 2). Average traces from these patches (Fig. 3 *A*), measured as the mean amplitudes during the final 100 ms of the pulse, were 12.13 *f*A for $\alpha_{1C}\beta_{1a}$ and 46.32 *f*A for $\alpha_{1C}\beta_{2a}$. This fourfold change compares well with the difference in macroscopic currents recorded at 0 mV. Since there is no change in single-channel conductance, this finding indicates that the $\alpha_{1C}\beta_{2a}$ subunit combination yields channels with a larger P_o than with $\alpha_{1C}\beta_{1a}$. Assuming that individual openings contribute 1.3 *p*A and all records contained only one active channel, the average P_o would then be 0.009 for $\alpha_{1C}\beta_{1a}$ and 0.036 for $\alpha_{1C}\beta_{2a}$. Estimating the number of active channels from patches with such a low P_o is virtually impossible. However, in the Discussion we will argue that records containing two channels are more likely to have been included in the $\alpha_{1C}\beta_{1a}$ data set and in such case the difference in P_o would be underestimated. On the other hand, macroscopic currents normalized by charge movement were also about fourfold larger for $\alpha_{1C}\beta_{2a}$ than for $\alpha_{1C}\beta_{1a}$ at 0 mV.

Single-channel activity recorded in oocytes shared several features characteristic of native cardiac Ca^{2+} channels exposed to the agonist S(−)Bay K 8644 (Hess et al., 1984): repeated depolarization often failed to evoke channel openings (nulls) and the P_o for traces with openings appears to fall in two classes reminiscent of the high and low P_o modes (Fig. 2). In one mode of gating (Low P_o), traces displayed brief and isolated openings whereas multiple bursts of openings characterized traces of the other mode (High P_o). Both modes of gating were observed in patches from oocytes expressing $\alpha_{1C}\beta_{1a}$ and $\alpha_{1C}\beta_{2a}$. The existence

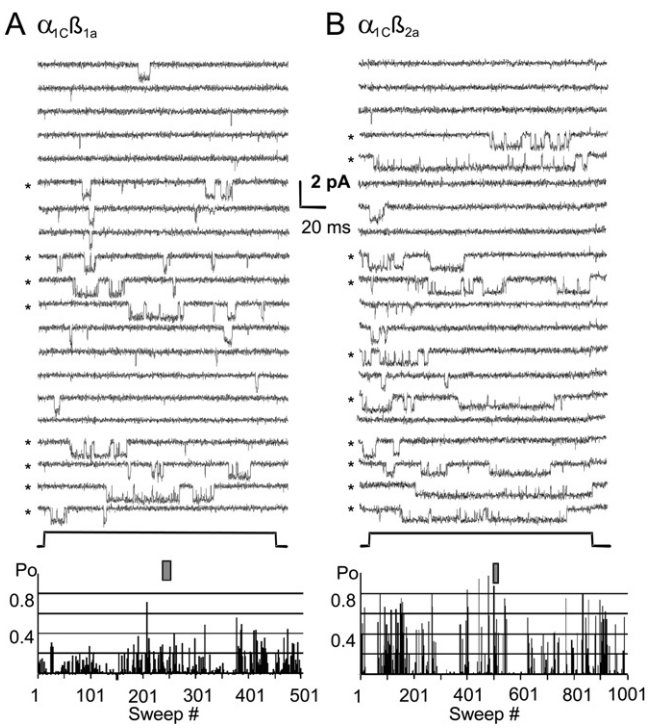

FIGURE 2 Single-channel recordings (*top*) and dairy plots (*bottom*) from oocytes expressing either $\alpha_{1C}\beta_{1a}$ (*A*) or $\alpha_{1C}\beta_{2a}$ (*B*). The patch from the oocyte expressing $\alpha_{1C}\beta_{1a}$ was interrupted after 500 traces whereas 1000 traces were collected from the oocyte expressing $\alpha_{1C}\beta_{2a}$. Traces with $P_o >$ 0.1 are labeled by *. Shaded rectangles over the dairy plots point to traces selected for display. Channels were activated at 1 Hz by 185-ms pulses to 0 mV from a holding potential of −70 mV. Recordings were sampled at 20 kHz and filtered at 2 kHz.

of gating modes was confirmed by run analysis as described in Horn et al. (1984). For single-channel patches with >20% of active traces, the standardized random variable Z was larger than the critical value (1.64) expected for a random distribution ($P \leq 0.05$) with both subunit combinations.

To sort out the extent to which changes in gating modes or in gating within each mode contributed to this difference, we compared the P_o distributions through P_o histograms combining all traces. Although we found a high degree of overlap (Fig. 3 *B*), the Mann-Whitney-Wilcoxon test (Bancroft and Han, 1981) indicates that there is more than a 95% probability that the two histograms originated from different populations and that P_o for β_{2a} is higher than for β_{1a}. The average P_o calculated from these histograms yields 0.008 ± 0.003 for $\alpha_{1C}\beta_{1a}$ and 0.020 ± 0.007 for $\alpha_{1C}\beta_{2a}$. We also noted that the sum of two exponential distributions approximated the P_o distributions and thus resorted to logarithmic binning to resolve different gating modes. Indeed, with this transformation, P_o histograms of active traces appear clearly bimodal, with a peak at low $P_o \sim 0.003$ for both subunit combinations, and a second peak at 0.1 for $\alpha_{1C}\beta_{1a}$ and at 0.2 for $\alpha_{1C}\beta_{2a}$ (Fig. 3 *C*). Also, the relative frequency of traces with $P_o > 0.1$ was severalfold larger for $\alpha_{1C}\beta_{2a}$ (18.0 ± 2.3%) than for $\alpha_{1C}\beta_{1a}$ (4.4 ± 1.6%),

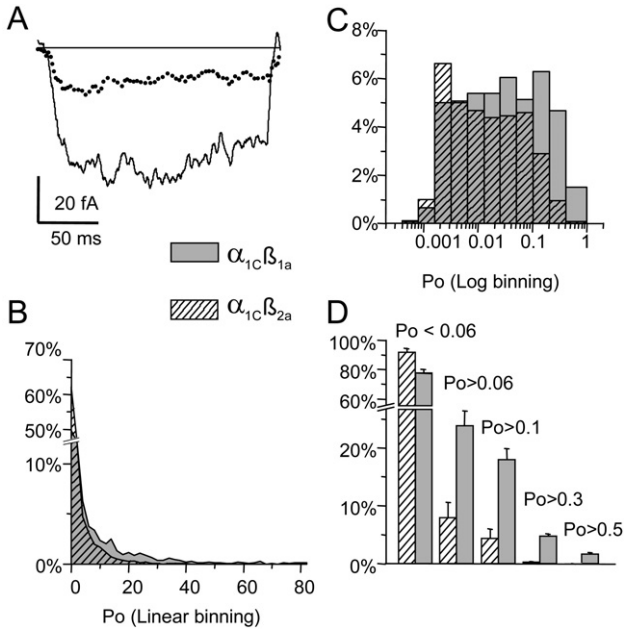

FIGURE 3 Mean current and P_o distribution from oocytes expressing $\alpha_{1C}\beta_{1a}$ (*cross-hatched*) and $\alpha_{1C}\beta_{2a}$ (*shaded*) subunits. (*A*) Mean current traces constructed with 2628 traces from seven single-channel patches from four oocytes expressing $\alpha_{1C}\beta_{1a}$ (*dotted line*) and 1514 traces from four single-channel patches from four oocytes expressing $\alpha_{1C}\beta_{2a}$ (*continuous line*). Traces were smoothed by averaging of window of 5 ms. (*B*) P_o frequency histograms constructed from the same records used in *A* expressed as a percent of the total number of traces. (*C*) P_o frequency histograms as in *B* but using logarithmic binning. (*D*) Cumulative P_o distributions. For $\alpha_{1C}\beta_{2a}$, on average, 77.4 ± 3.1% of the traces have $P_o \leq 0.06$, while 23.8 ± 3.1% have $P_o > 0.06$; 18.0 ± 1.9% $P_o > 0.1$; 4.8% ± 0.3% $P_o > 0.3$; and 1.7 ± 0.3% $P_o > 0.5$. For $\alpha_{1C}\beta_{1a}$, 92.0 ± 2.7% of the traces have $P_o \leq 0.06$, while 8.0 ± 2.7% of the traces have $P_o > 0.06$; 4.4 ± 1.6% $P_o > 0.1$; 0.3 ± 0.1% $P_o > 0.3$; and 0.03 ± 0.03% $P_o > 0.5$. The differences are statistically significant for all bins in *D* ($P < 0.05$, two-tailed *t*-test).

whereas traces with no or very low activity ($P_o \leq 0.06$) were more frequent with $\alpha_{1C}\beta_{1a}$ (92.0 ± 2.7%) than with $\alpha_{1C}\beta_{2a}$ (77.4 ± 3.1%; Fig. 3 *D*). These results indicate that increased frequency of high P_o sweeps contribute to the augmented currents observed in oocytes expressing $\alpha_{1C}\beta_{2a}$.

Unfortunately, patch-to-patch variability, the relatively short duration of runs and difficulties in separating each mode, prevented us from establishing whether this increase is due to a higher chance of entering the high P_o mode or larger stability of this state. On the other hand, the shift in the mode of the high P_o sweeps revealed in the log-binned P_o histograms suggests that channel kinetics within gating modes may also contribute to increases in P_o mediated by co-expression of β_{2a}.

Dwell-time histograms

For the analysis of dwell-times, recordings from patches with a few isolated double openings were also included to improve our estimates of mean open times and MBD by raising the number of experiments to 14 for $\alpha_{1C}\beta_{2a}$ and 12 for $\alpha_{1C}\beta_{1a}$. However, the lifetime of long closed states may be underestimated, since even for sweeps without overlapping openings there is a chance that two channels became active simultaneously. Another shortcoming of adding patches known to have more than one channel is that sweeps selected by mode may also include some activity of channels in different modes. Bearing these limitations in mind, only the changes in the major components of dwell-time histograms were considered.

Open-time histograms constructed with all traces in a recording often required the sum of up to three exponential distributions to adequately describe the data, even for channels with seemingly mono-modal P_o distribution (Fig. 4). On the other hand, contribution of brief openings ($\tau_{fast} <$ 0.5 ms) to open-time histograms was greatly reduced, and often no longer detectable when traces with $P_o \leq 0.1$ were excluded, even for clearly bimodal channels, as illustrated in Fig. 4. Average time constants and relative amplitudes of each component for histograms constructed with all traces or only with traces with $P_o > 0.1$ or $P_o \leq 0.1$ are summarized in Table 2. We only found a significant difference in the time constant of the fast component measured in the histograms built from traces with $P_o > 0.1$. However, this component turns out to be shorter for $\alpha_{1C}\beta_{2a}$ (1.54 ± 0.33 ms compared to 2.60 ± 0.56 ms for $\alpha_{1C}\beta_{1a}$) and thus, would contribute to a decrease in P_o for $\alpha_{1C}\beta_{2a}$. We also noted that events with open-time < 0.6 ms were more frequent than predicted by the exponential distributions, suggesting that the combined effect of noise and limited bandwidth was giving rise to nonexponential distributions (McManus et al., 1987). This problem was further aggravated by the small number of events in each recording (562 ± 177 and 1402 ± 299 events for $\alpha_{1C}\beta_{1a}$ and $\alpha_{1C}\beta_{2a}$, respectively). As an alternative, we compared the time constants defining the single exponential distribution that best described the open-time histograms constructed from traces with $P_o > 0.1$. With this simplification, we were able to detect a modest (26%) but statistically significant increase in τ_{open} with β_{2a} (Table 4).

A minimum of two exponential distributions was necessary to describe closed-time histograms, and sometimes a third component of intermediate duration could be detected. If only closures from traces with a $P_o > 0.1$ were selected, the intermediate component could seldom be resolved. The simplest interpretation for this complexity is that closing events arising from low P_o gating mode were not eliminated completely by selecting traces with $P_o > 0.1$, as would happen when channels switched mode within a trace. However, this source of error should affect, to a similar extent, the measurements obtained with both β-subunits, and a simplified model should increase our ability to detect differences. Here we limited the number of exponential components to two. Fig. 5 compares closed-time histograms from the same patches used for the open-time histograms shown in Fig. 4. With this simplification, we identified two

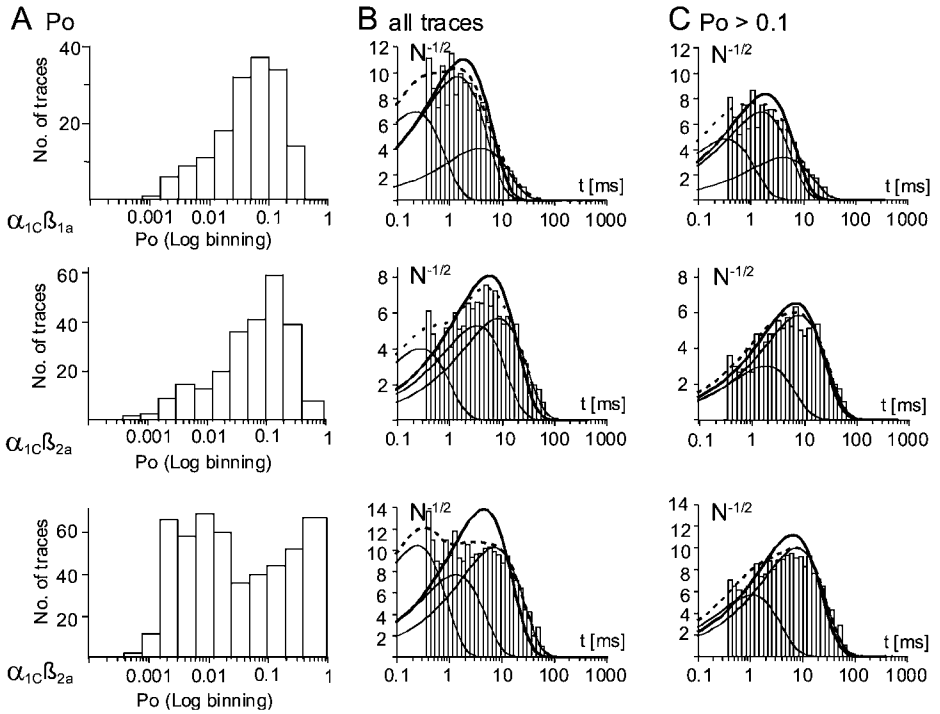

FIGURE 4 Open-time histograms and P_o distributions from oocytes expressing $\alpha_{1C}\beta_{1a}$ and $\alpha_{1C}\beta_{2a}$. (*A*) P_o histograms with logarithmic binning from an oocyte expressing $\alpha_{1C}\beta_{1a}$ (*top*). The middle and bottom panels illustrate two $\alpha_{1C}\beta_{2a}$ examples that differ in the relative contribution of low P_o traces. (*B*) Open-time histograms using all traces, and (*C*) open-time histograms from traces with $P_o > 0.1$. Histograms were fitted by a single exponential distribution (*thick lines*) or to the sum of two or three components (*dashed lines*). The thin lines show the contribution of individual exponential distributions. See Table 4 for parameters used.

well-separated closed states whose mean lifetimes do not appear to be modulated differentially by the different β-subunits.

Burst-durations analysis

A potential mechanism that may increase the P_o within a gating mode is by reducing the exit rate to long-lived closed states. This should be reflected in an increase in MBD. Burst-duration histograms for patches from oocytes expressing $\alpha_{1C}\beta_{1a}$ or $\alpha_{1C}\beta_{2a}$ are compared in Fig. 6. When all traces were included in the analysis, often single exponential distributions did not yield an adequate fit (Fig. 6 *C*), whereas burst-duration histograms from traces with $P_o > 0.1$ appeared well-described by single exponential distributions (Fig. 6, *A* and *B*, and Table 4). The time constant defining this single exponential distribution was taken as the MBD. For a few patches, we systematically varied the minimum P_o of the traces included in the burst-duration histograms and found no changes in MBD from $P_o > 0.05$ to $P_o < 0.3$; selecting sweeps with higher P_o resulted in a sharp increase in MBD. We also found that adding a second exponential component improved the quality of the fit only marginally, and the duration of the slowest component remained within 15% of the time constant obtained from the fit with a single exponential distribution. The slow component of double-exponential distributions used to adjust burst-duration histograms from all traces had average time constants of 9.5 ± 1.1 ms and 12.0 ± 1.0 ms for $\alpha_{1C}\beta_{1a}$ and $\alpha_{1C}\beta_{2a}$, respectively.

Mean burst-durations with other subunit combinations

One important issue that we needed to address was whether heterogeneity in the subunit composition was responsible for

TABLE 1 Parameters used for Fig. 4

	DN60β_{1a} (*top*)		DN60β_{2a} (*middle*)		DN60β_{2a} (*bottom*)	
	All sweeps	$P_o > 0.1$	All sweeps	$P_o > 0.1$	All sweeps	$P_o > 0.1$
τ_{open}	3.74	4.10	5.74	7.54	6.78	8.52
τ_{short}	NS	NS	1.17	NS	1.01	NS
A_{short}	NS	NS	0.40	NS	0.21	NS
τ_{medium}	1.85	2.91	2.20	1.84	4.38	2.84
A_{medium}	0.38	0.59	0.22	0.24	0.37	0.21
τ_{long}	4.68	5.60	8.83	8.94	9.90	9.86
A_{long}	0.62	0.41	0.39	0.76	0.42	0.79

τ_{open} refers to the time constant when the histograms were fitted to a single exponential distribution. *NS* indicates that this component did not improve the fit significantly or that there was no convergence.

TABLE 2 Multiexponential distributions describing open-time histograms for $\alpha_{1C}\beta_{1a}$ and $\alpha_{1C}\beta_{2a}$

		τ_1 (ms)	A_1	τ_2 (ms)	A_2	τ_3 (ms)	A_3
	All traces	0.67 ± 0.06	0.50 ± 0.05	2.58 ± 0.33	0.28 ± 0.05	9.35 ± 2.45	0.14 ± 0.03
$\alpha_{1C}\beta_{1a}$	$P_o > 0.1$			2.60 ± 0.56*	0.42 ± 0.07	7.26 ± 1.12	0.58 ± 0.07
($n = 14$)	$P_o \leq 0.1$	0.82 ± 0.07	0.67 ± 0.04	2.78 ± 0.18	0.33 ± 0.04		
	All traces	0.58 ± 0.02	0.47 ± 0.06	3.11 ± 0.35	0.32 ± 0.05	10.2 ± 1.41	0.21 ± 0.06
$\alpha_{1C}\beta_{2a}$	$P_o > 0.1$			1.54 ± 0.33*	0.35 ± 0.06	7.08 ± 0.87	0.65 ± 0.05
($n- = 12$)	$P_o \leq 0.1$	0.76 ± 0.04	0.65 ± 0.04	3.10 ± 0.39	0.36 ± 0.04		

Mean ± SE of parameters defining multiple exponential distributions that best fitted open-time histograms from individual patches. The sum of three exponential distributions was used to adjust histograms derived from all traces regardless of the significance of the third component. Only two exponential distributions were added to fit open-time histograms from traces selected according to their P_o. Only τ_2 from traces with $P_o > 0.1$ were significantly different for the two subunit combinations (*$P < 0.05$; two-tailed t-test).

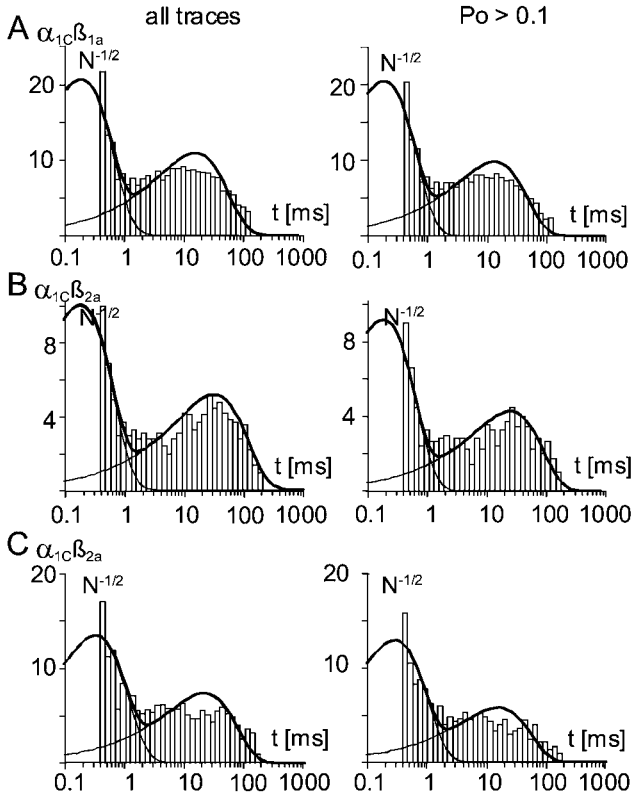

FIGURE 5 Closed-time histograms from oocytes expressing $\alpha_{1C}\beta_{1a}$ and $\alpha_{1C}\beta_{2a}$. Same patches as in Fig. 4 with *A* and *B* corresponding to patches showing a single peak in the P_o frequency histogram and *C* from the oocyte expressing $\alpha_{1C}\beta_{2a}$ in which the P_o frequency histogram reveals two modes of activity. The left panel shows a closed-time histogram using all traces, whereas in the right panel only traces with $P_o > 0.1$ were selected. The sum of two exponential distributions was used to fit the data (*thick line*). The thin lines show the contribution of individual exponential distributions. See Table 3 for parameters used.

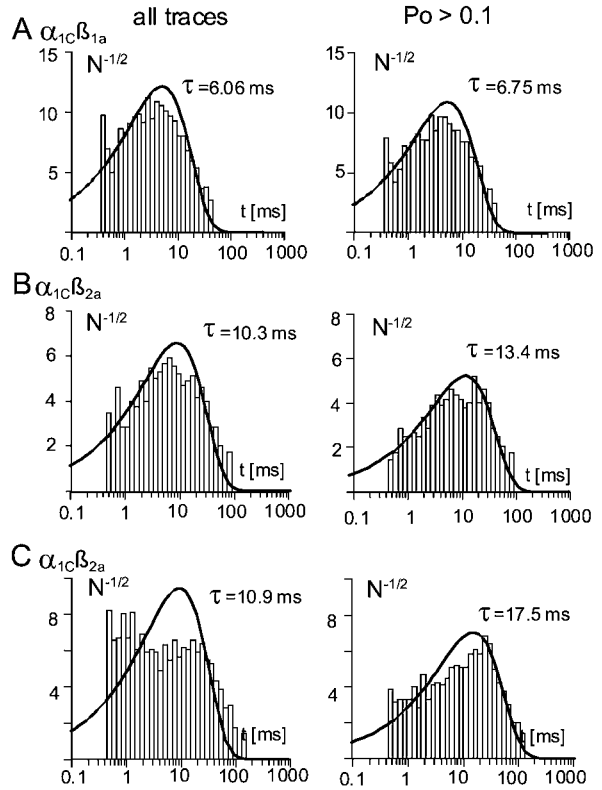

FIGURE 6 Burst-duration histograms from oocytes expressing $\alpha_{1C}\beta_{1a}$ and $\alpha_{1C}\beta_{2a}$. Burst-duration histograms from all traces (*left*) are compared to histograms containing only burst from traces with $P_o > 0.1$ (*right*). Same patches as in Figs. 4 and 5. Patches in which the distribution of P_o show a single peak (*A* and *B*), burst-durations followed a single exponential distribution when either all or only $P_o > 0.1$ traces are included. In contrast, burst-durations histograms from patches with two modes of activity can be described by a single exponential distribution only when traces with $P_o > 0.1$ are used (*C*). Time constants (*ms*) defining the exponential distribution that best fitted the data are shown next to each histogram.

TABLE 3 Parameters used for Fig. 5

	DN60β_{1a} (*A*)		DN60β_{2a} (*B*)		DN60β_{2a} (*C*)	
	All sweeps	$P_o > 0.1$	All sweeps	$P_o > 0.1$	All sweeps	$P_o > 0.1$
τ_{short} (ms)	0.91	0.89	0.90	0.84	1.05	1.01
A_{short}	0.78	0.81	0.79	0.83	0.77	0.83
τ_{long} (ms)	18.50	15.59	31.14	27.12	25.12	18.07

TABLE 4 Dwell-times from oocytes expressing either $\alpha_{1C}\beta_{1a}$ or $\alpha_{1C}\beta_{2a}$

	$\alpha_{1C}\beta_{1a}$ ($n = 14$)	$\alpha_{1C}\beta_{2a}$ ($n = 12$)
Open times (ms)	4.98 ± 0.20	6.25 ± 0.42†
Short closed times (ms)	0.88 ± 0.06	0.78 ± 0.05
Long closed time (ms)	22.2 ± 1.84	21.5 ± 1.48
Fraction of long closures (ms)	0.32 ± 0.03	0.36 ± 0.03
Burst durations (ms)	8.40 ± 0.53	15.07 ± 0.71*

Mean ± SE for parameters describing open-times, closed-times, and burst-duration histograms from oocytes expressing either $\alpha_{1C}\beta_{1a}$ or $\alpha_{1C}\beta_{2a}$. All histograms were constructed from traces with $P_o > 0.1$. A single exponential distribution was adjusted to the open-time and burst-duration histograms. The sum of two exponential distributions was used to fit the closed-time histograms. The mean burst durations and mean open times were significantly different for the two subunit combinations (*$P < 0.01$ and †$P < 0.05$ for two-tailed t-test).

the observed difference in MBD. For instance, in some patches, channel activity could arise from an α_{1C} subunit combined with an endogenous β-subunits (β_{3xo}). In this case the likelihood of recording patches with β_{3xo} could be higher if cRNA encoding β_{1a} expressed less efficiently than cRNA encoding β_{2a}. In this scenario, a decrease in MBD could result from an increased contribution of $\alpha_{1C}\beta_{3xo}$ rather than from functional differences between β_{2a} and β_{1a}. Alternatively, if two or more β-subunits interact with the channel-forming subunit (Tareilus et al., 1997), α_{1C} channels coupled to a single β may display shorter MBD and channels with a reduced subunit complement may predominate with one of the β-isoforms. To sort out these possibilities, we investigated the behavior of Ca^{2+} channels expressed in oocytes injected with cRNA encoding α_{1C} alone and combined with cRNA encoding either β_{3xo} or a splice-variant of β_1 (β_{1b}). Example traces and burst histograms from traces with $P_o > 0.1$ are shown in Fig. 7 and dwell-time parameters are summarized in Table 5. The $\alpha_{1C}\beta_{3xo}$ channels display long bursts (14.3 ± 1.1 ms) ranging from 10.9 ms to 15.9 ms, whereas MBD from six patches out of three oocytes injected with α_{1C} cRNA alone ranged from 3.74 to 4.51 ms (4.7 ± 0.1 ms). This difference indicates not only that α_{1C} alone can support channel activity but also rules out the possibility that intermediate MBD arises from α_{1C} combined with the endogenous β or with an incomplete set of β. On the other hand, channels from oocytes co-expressing β_{1b} with α_{1C} display a MBD of 8.2 ± 0.5 ms, virtually the same as that for $\alpha_{1C}\beta_{1a}$. It is unlikely that expression efficiency would be equally reduced for these two splice-variants of different length. A more plausible explanation is that structural features of the β-subunit confer the different MBD phenotypes.

Opening and closing rates from all-points histograms

Having established that the β-subunit modulates the MBD of Ca^{2+} channels in an isoform-dependent manner, we sought the identification of the specific conformations and transitions being affected. MBD may be increased by longer open-times, increasing the rate of re-opening (shorter brief closures) or slower transitions to long-lived closed states. As long as all events are detected and measured accurately, all these parameters can be obtained directly from dwell-time histograms and historically, open-times for Ca^{2+} channels measured in the presence of Bay K 8644 have been assumed to be well-resolved and to last several ms. However, little consideration has been paid to missed closed events even though the reported lifetimes for brief closures are below or near the filter's dead time at 1 kHz (Hess et al., 1984; Lacerda and Brown, 1989; Marks and Jones, 1992). For

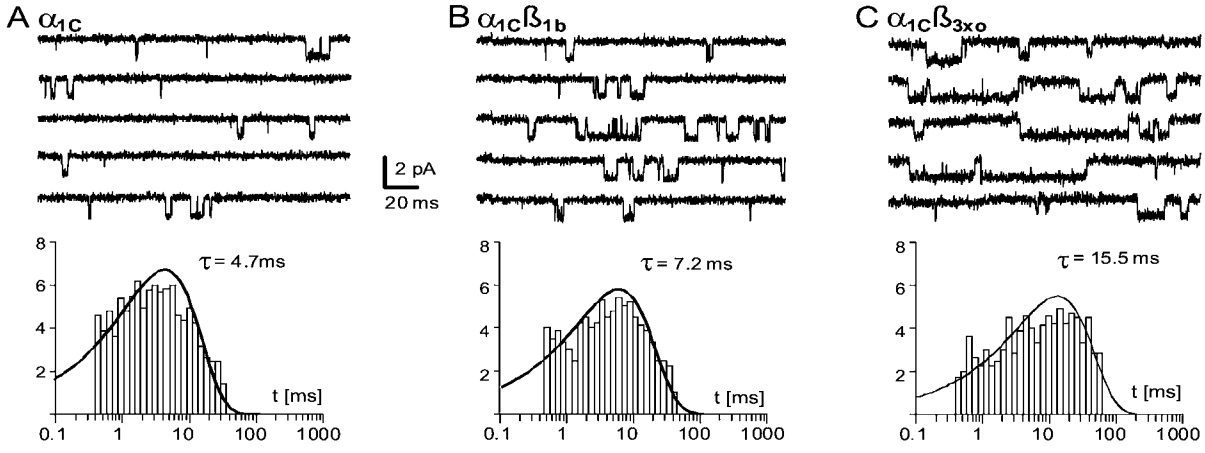

FIGURE 7 Burst-duration histogram from oocytes expressing α_{1C} alone or combined with β_{1b} or β_{3xo}. Representative traces (*top*) and burst-duration histograms from traces with $P_o > 0.1$ (*bottom*) of patches containing a single channel from *Xenopus* oocytes injected with mRNA encoding the α_{1C} subunit alone (*A*), combined with mRNA for β_{1b} (*B*) or for β_{3xo} (*C*). Continuous lines depict the single exponential distributions that best fitted the burst-duration histograms; the time constants (ms) are shown next to each plot.

TABLE 5 Dwell-times from oocytes expressing α_{1C}, $\alpha_{1C}\beta_{3XO}$ or $\alpha_{1C}\beta_{1b}$

	α_{1C} ($n = 6$)	$\alpha_{1C}\beta_{1b}$ ($n = 5$)	$\alpha_{1C}\beta_{3xo}$ ($n = 5$)
Open times (ms)	2.85 ± 0.25	4.48 ± 0.59*	6.48 ± 0.63*
Short closed times (ms)	0.87 ± 0.13	0.86 ± 0.11	0.80 ± 0.03
Long closed times (ms)	18.7 ± 1.59	25.4 ± 3.89	22.5 ± 1.52
Fraction of long closures	0.61 ± 0.04	0.43 ± 0.05*	0.42 ± 0.03*
Burst durations (ms)	4.67 ± 0.12	8.19 ± 0.45*	14.31 ± 1.07*

Mean ± SE for parameters describing open-times, closed-times, and burst-durations histograms from oocytes expressing α_{1C}, $\alpha_{1C}\beta_{1b}$, or $\alpha_{1C}\beta_{3xo}$. All histograms were constructed from traces with $P_o > 0.1$. A single exponential distribution was adjusted to the open-time and burst-durations histograms and the sum of two exponential distributions was used to fit the closed-time histograms. With the two β-subunits, mean burst durations, open times, and the fraction of long closures were significantly different from data obtained from oocytes injected with α_{1C}-mRNA injected by itself (*$P < 0.01$ for a two-tailed t-test).

a simple two-states model and a 50% threshold detection algorithm, the true mean lifetime of the open state ($\tau_{true(O)}$) can be calculated from the observed mean lifetime ($\tau_{obs(O)}$), the fraction of detected shut intervals ($F_{det(S)}$), and the mean lifetime of missed shut intervals ($T_{miss(S)}$), taking into consideration the dead time (T_d) of the recording, according to McManus and co-workers (1987):

$$\tau_{obs(0)} = \frac{\tau_{true(0)} + (1 - F_{det(S)}) \times T_{miss(S)}}{F_{det(S)}}, \quad (4)$$

where

$$F_{det(S)} = \exp(-T_d/\tau_{true(S)}), \quad (5)$$

and

$$T_{miss(S)} = \frac{\tau_{true(S)} - (\tau_{true(S)} - T_d) \times \exp[-T_d/\tau_{true(S)}]}{(1 - \exp[-T_d/\tau_{true(S)}])}. \quad (6)$$

By reversing S and O, a similar set of equations yields $\tau_{true(O)}$ and $\tau_{true(S)}$.

Assuming $T_d = 0.1$ ms and $\tau_{obs(O)}$ and $\tau_{obs(S)}$ from Table 4 (open-time and short closed-time respectively), we numerically solved the complete set of equations for $\alpha_{1C}\beta_{1a}$ and $\alpha_{1C}\beta_{2a}$. As expected, two sets of solutions were obtained for each subunit combination; for $\alpha_{1C}\beta_{1a}$, $\tau_{true(O)}$ and $\tau_{true(S)}$ can take the values of 4.10 ms and 0.66 ms or 0.039 ms and 0.023 ms, respectively, whereas $\alpha_{1C}\beta_{2a}$, 5.07 ms and 0.57 ms, or 0.041 ms and 0.022 ms, constitute solutions for $\tau_{true(O)}$ and $\tau_{true(S)}$, respectively. To determine which of the two possible solutions is a better approximation of $\tau_{true(O)}$ and $\tau_{true(S)}$, we used the distribution of current amplitudes within a burst of openings (APDF) to obtain a detection-independent estimate of the channel opening and closing rate (Pietrobon et al., 1989; Prodhom et al., 1989; Villarroel et al., 1988; Yellen, 1984). Here, to simplify the analysis we neglected the contributions from transitions at the beginning and end of bursts and constructed all-points histograms from whole traces with $P_o > 0.1$ (see Methods). One of the advantages of this approach is that information on baseline noise can be extracted from the same histogram. Fig. 8 compares APDF from two patches expressing $\alpha_{1C}\beta_{1a}$ and $\alpha_{1C}\beta_{2a}$, chosen for having the same baseline noise and open-channel current amplitudes, and shows that they are nearly identical. This match suggests that opening and closing rates for both subunit combinations are the same. To extract opening and closing rates from APDF, we systematically varied k_O and k_C and found that when the ratio k_O/k_C was kept at 10 and $k_O > 10{,}000\ s^{-1}$, $A(x)$ fit the experimental APDF extremely well. The thick line in Fig. 8 *C* corresponds to $A(x)$ when $k_O = 25{,}000\ s^{-1}$ and $k_C = 2500\ s^{-1}$. This indicates that $\tau_{true(S)}$ and $\tau_{true(O)}$ are near 10-fold shorter than predicted by dwell-time histograms, and also that the P_o within bursts is close to 0.9. The latter would also be consistent with the slowest solution of $\tau_{true(S)}$ and $\tau_{true(O)}$ for $\alpha_{1C}\beta_{2a}$ ($k_O = 1762\ s^{-1}$ and $k_C = 197\ s^{-1}$), but $A(x)$ is visibly sharper than the data (*thin line* in Fig. 8 *C*). On the other hand, the fast solution ($k_O = 43{,}478\ s^{-1}$ and $k_C = 25{,}651\ s^{-1}$) yields a rather wide and symmetrical $A(x)$ that reaches a maximum near a normalized amplitude of 0.6 that is inconsistent with the expected P_o within bursts (not shown). From these comparisons, it would appear, then, that $\tau_{true(S)}$ and $\tau_{true(O)}$ are near 10-fold shorter than predicted by dwell-time histograms, and cannot be corrected for by the equations proposed for a two-states model.

Modeling and simulations

To further evaluate whether opening and closing rates were as fast as suggested by the APDF, we studied the behavior of one of the simplest model, that gives rise to bursts of openings: a sequence of three states with a final opening where a series of fast transitions between C_1 and O are terminated by a transition to a long-lived closed state (C_2).

$$C_2 \underset{k_{-1}}{\longleftarrow} C_1 \underset{k_C}{\overset{k_O}{\rightleftarrows}} O. \quad (7)$$

In this case, the MBD depends on the rate connecting C_1 to C_2 (k_{-1}) and the relative time spent on C_1 according to the following equation (Colquhoun and Hawkes, 1981):

$$MBD = \frac{1}{k_C}\left(1 + \frac{k_O}{k_{-1}}\right) + \frac{k_O}{k_{-1}}\left(\frac{1}{k_O + k_{-1}}\right). \quad (8)$$

Assuming $k_O = 25{,}000\ s^{-1}$ and $k_C = 2500\ s^{-1}$, as in the

APDF that fitted the data in Fig. 8 *C* (*continuous line*), this equation predicts that an exit rate to long-lived closed state (k_{-1}) of 748 s^{-1} yields a MBD of 15.1 ms, as the one measured for $\alpha_{1C}\beta_{2a}$. MBD can be shortened to 8.40 ms, like $\alpha_{1C}\beta_{1a}$, by increasing k_{-1} to 1369 s^{-1}. The same change in MBD should be obtained if k_O is reduced to 12,597 s^{-1} or k_C is raised to 4848 s^{-1}. However, in both cases the predicted APDF from a two-states model visibly deviates from the experimental data (Fig. 8 *C*). These large changes in the shapes of the APDF can be intuitively foreseen since, in contrast to modifying the transition rate out of the burst, decreasing the opening rate or increasing the closing rate by 50% will go along with large changes in the P_o and the number of transitions within a burst. Thus, the similarity of APDF for both subunit combinations indicates that the exit rate to the long-lived closed state is the chief transition being modulated differentially by the two β-subunits whereas fast openings and closing within a burst remain virtually unchanged.

The issue to be addressed now is whether channels with opening and closing rates 10-fold faster than the system's dead-time yield dwell-time histograms with apparent open-time in the ms range. To this end, we simulated single-channel activity using the same sampling rate, filter, and noise as in the recordings. These simulations were then analyzed using the same detection parameters as for the experimental data, and dwell-time and burst-duration histograms were constructed from traces with $P_o > 0.1$. We tested the different values of k_O, k_C, and k_{-1} that mimic the changes in MBD. The forward rate between C_2 and C_1 (k_1) was set at 50 s^{-1} to approximate the value obtained from closed-time histograms. Representative traces and burst-duration histograms of simulated channels are shown in Fig. 9. Single-channel activity from these simulations was characterized by burst of openings lasting several ms and traces within bursts appeared with increased noise. For the rates chosen to mimic $\alpha_{1C}\beta_{2a}$ activity, the measured MBD were remarkably close to the calculated value (15.2 ms). Also simulation with k_O, k_C, or k_{-1} modified individually to reduce the MBD to 8.4 ms produced burst-duration histograms with mean values that approached the expected value. It is noteworthy that, in all cases, very few shut intervals could be resolved within a burst, illustrating how one can be easily misled to conclude that all openings are well-resolved. On the other hand, despite the fact that most brief closures go undetected, burst-durations histograms appear to be accurate. This stands in contrast with open-time histograms that predict lifetimes an order-of-magnitude longer than expected from the closing rates used in the simulation (Fig. 10). Interestingly, open-time histograms from the simulated data labeled β2a and β1a_1 were nearly identical to the experimental data from $\alpha_{1C}\beta_{2a}$ and $\alpha_{1C}\beta_{1a}$, respectively. Moreover, even though closing and opening rates were the same in these two simulations, τ_{open} decreases from 5.44 ms (β2a) to 4.81 ms (β1a_1; Fig. 10 *A*); a difference that compares with the one that separates $\alpha_{1C}\beta_{2a}$ from $\alpha_{1C}\beta_{1a}$. These simulations also show that slowing the opening rate (β1a_2) or increasing the closing rate (β1a_3) by near twofold to reduce the MBD, shortens the apparent τ_{open} significantly and should have been detected experimentally. Changing these rates also has a significant impact in the APDF (Fig. 10 *C*). For comparison, we also included the distribution (*continuous line*) that fit the experimental APDF in Fig. 8 *C*; it nearly perfectly superimposes to the APDF from simulation β2a and β1a_1. The only deviations occur at lower amplitude bins where transitions to and from long closures come into

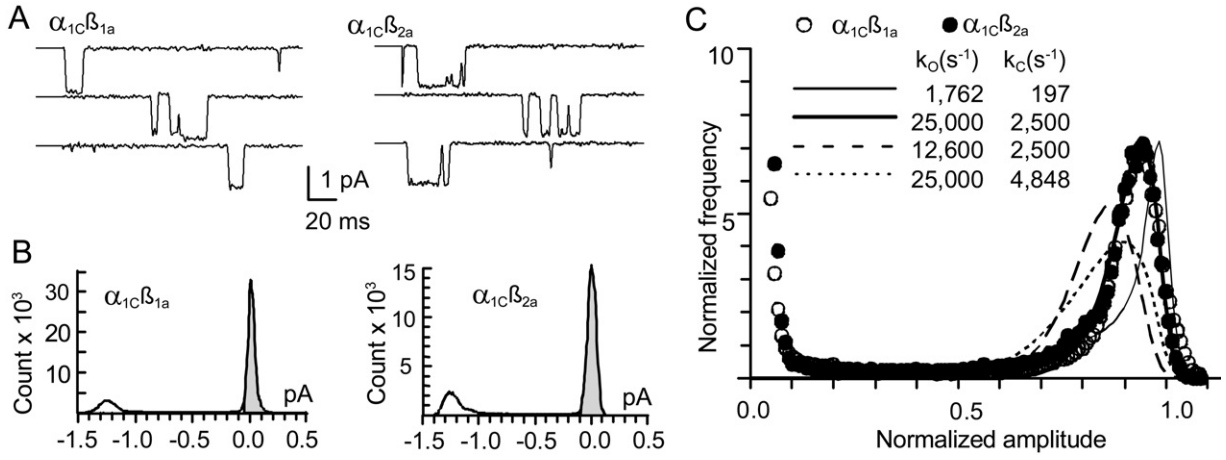

FIGURE 8 Open-channel amplitudes PDF. (*A*) Representative traces from on-cell patches after digitally filtering at 300 Hz and eliminating capacitive transients and baseline fluctuations (see Methods). The left and right panels are from oocytes expressing $\alpha_{1C}\beta_{1a}$ and $\alpha_{1C}\beta_{2a}$, respectively. (*B*) All-points histograms from traces with $P_o > 0.1$. The baseline standard deviations, as defined by the Normal distributions that best fitted the baseline (*shaded area*), were 0.039 p_A and 0.041 p_A for $\alpha_{1C}\beta_{1a}$ and $\alpha_{1C}\beta_{2a}$, respectively. (*C*) APDF for $\alpha_{1C}\beta_{1a}$ (○) and $\alpha_{1C}\beta_{2a}$ (●). The continuous thick line depicts an $A(x)$ with k_C = 25,000 s^{-1} and k_O = 2500 s^{-1}. For comparison, we also included $A(x)$ distributions for different values for k_O and k_C, as indicated in this figure.

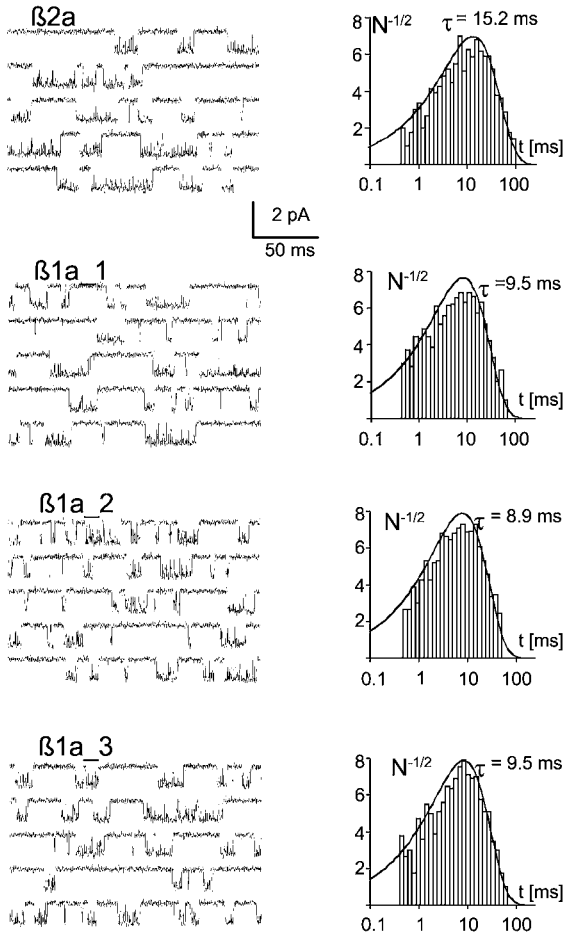

FIGURE 9 Simulated single-channel activity and burst-durations histograms. Single-channel activity was simulated assuming a three-states model as described in methods. Left panels show the first five consecutive traces of each simulation. Each simulation was ran for 128 traces and analyzed with TRANSIT using the same parameters as for the experimental data. See Table 6 for rates used. The time constants of the exponential distribution that best fitted the data is shown next to the respective histogram.

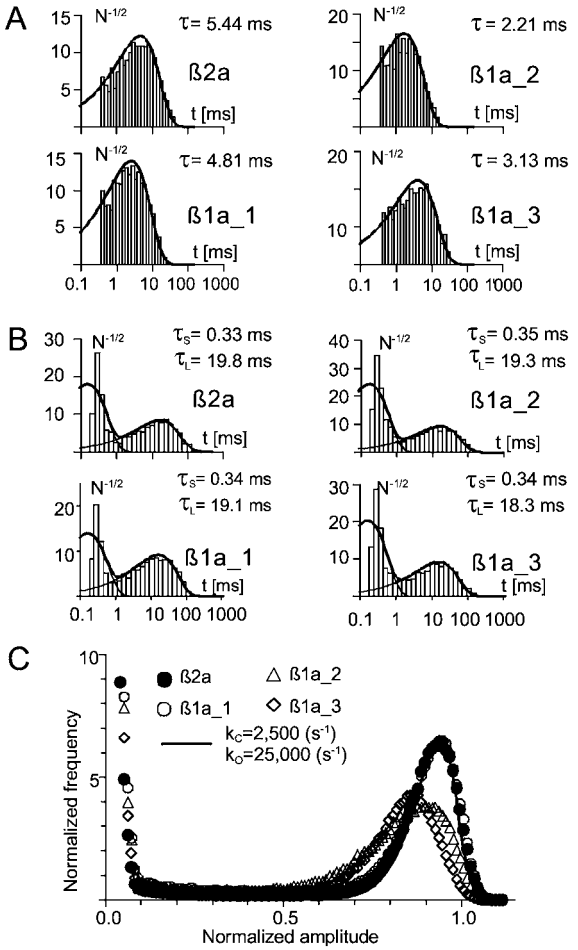

FIGURE 10 Dwell-time histograms and APDF from simulated channels. (*A*) Open-time histograms and (*B*) closed-time histograms generated from the simulated data. Single exponential distributions described open-time histograms whereas the sum of two exponential distributions was used to describe closed-time histograms. Time constants and relative contribution of each exponential distribution are shown next to each histogram. APDF from simulated channels is shown in *C*. The continuous line is the same $B(x)$ shown in Fig. 11 ($k_O = 25{,}000\ s^{-1}$ and $k_C = 2500\ s^{-1}$) convolved to the baseline noise of simulation labeled β_{2a}.

play. The effect of decreasing the opening rate ($k_O = 12{,}600\ s^{-1}$) or increasing the closing rate ($k_C = 4848\ s^{-1}$) on the APDF is illustrated by β1a_2 and β1a_3 data, respectively. In summary, the simulated data reproduces remarkably well the properties and differences of open-time histograms and APDF, and provide independent evidence for a large discrepancy between the true and measured dwell-times.

The simple three-states model discussed here is not intended to provide a full description of Ca^{2+} channel behavior, but rather to illustrate the fact that fast openings and closings may give rise to channel activity that, because of bandwidth limitations, appears to be well-resolved. In fact, there are some deviations from the experimental data suggesting that more states are involved. For instance, closed-time histograms consistently showed a fast component with a lifetime less than one-half the one from the experimental data. This situation cannot be corrected for by decreasing the opening rate by nearly 50% without visibly affecting open-time histograms and APDF (β1a_2 in Fig. 10 *C*). However, we were able to increase the apparent lifetime of the fast component of closed-time histograms by adding a closed state that followed channel opening. This closed state had a true lifetime of ~0.5 ms and a forward rate such that this state is visited once every 10

TABLE 6 Rates used for Fig. 9

	$k_O^{[s-1]}$	$k_C^{[s-1]}$	$k-1^{[s-1]}$	$K1^{[s-1]}$
β2a	25,000	2500	748	50
β1a_1	25,000	2500	1369	50
β1a_2	12,600	2500	748	50
β1a_3	25,000	4847	748	50

The τcrit to construct burst-duration histograms was set to 1 ms.

closures within a burst. In this new model, it also happens that changing opening and closing rates to decrease MBD affects the APDF visibly (not shown). We also explored the behavior of more complex models such as the one proposed by Costantin et al. (1998) with multiple open states connected to a single short-lived closed state. In this case, changing the gating kinetics inside the burst also leads to dramatic changes in the APDF, reinforcing the view that the β-subunit modulates transition to the long-lived closed state and that fast gating within the burst is governed by a separated mechanism.

DISCUSSION

The P_o is differentially modulated by the β-subunit

To gain new insights on the molecular mechanisms of channel activation we selected two β-subunits that, when combined with the cardiac α_{1C} subunit, yield Ca^{2+} channels with different coupling efficiency between voltage-sensing and pore-opening. We measured a difference in coupling efficiency of more than twofold between β_{1a} and β_{2a} when comparing the amplitude of ionic currents normalized by maximal charge movements. We also confirmed that single-channel conductances are the same with both subunits, indicating that a difference in P_o must be the culprit. This appears corroborated by the difference in the mean amplitude of average traces from single-channel recordings. However, the magnitude of such change is less certain, because some of the patches from $\alpha_{1C}\beta_{1a}$ expressing oocytes may have contained more than one channel, even if they never open simultaneously.

An upper limit on the likelihood of not observing double openings from patches with two channels can be estimated from the steady-state P_o. If two channels contributed to the P_o estimated for $\alpha_{1C}\beta_{2a}$ (0.036), then each channel should have a P_o of 0.018. In this case, the probability of observing a double opening at any given time should be $0.018^2 = 3.24 \times 10^{-4}$, and of not observing a double opening in 500 consecutive observations should be $(1 - 3.24 \times 10^{-4})^{500} > 0.80$. In other words, there is an 80% chance of not observing a double opening in 500 consecutive trials in a two-channels patch if the P_o of each individual channel is 0.018. However, this approach does not consider that during each sweep each channel may have several opportunities of reaching the open state. For example, if each channel opens on average 100 times per sweep, the likelihood of not observing a double would be $(1 - 3.24 \times 10^{-4})^{100} = 0.97$ and, in 500 sweeps the likelihood becomes $0.97^{500} < 10^{-7}$. Here, we do not have previous knowledge on how many times a channel opens in a sweep and how many sweeps contain openings. So we approached this issue by simulating several models based on the most reliable information derived from our experiments. In these simulations, 50,000 sweeps were generated in each run and sweeps containing double openings were counted to estimate the probability of observing double openings. Each model was run several times to estimate an error on the number of double openings counted. We consistently found that in models in which more than 12% of the sweeps had each channel staying open at least 10% of the time ($P_o > 0.1$), the likelihood of not observing double openings in 500 sweeps is less than 1%. Considering that for $\alpha_{1C}\beta_{2a}$, 18 ± 2% of the sweeps had $P_o > 0.1$ it is unlikely that patches containing two channels were included in this analysis. On the other hand, in simulations that yield less than a 7% of sweeps with $P_o > 0.1$, the chances of not observing double openings in two-channels patches surpassed 20%. Thus, it is not unlikely that patches form oocytes expressing $\alpha_{1C}\beta_{1a}$, having less than 5% of the sweeps with $P_o > 0.1$, may have held more than one channel. If this is the case, the differences in amplitude in mean currents we observed may be smaller than the true difference in P_o between the two subunit combinations.

Modulation of fast and slow gating

Single-channel activity underlying the expression of $\alpha_{1C}\beta_{2a}$ and $\alpha_{1C}\beta_{1a}$ displayed fluctuations in the P_o, suggesting that these channels, like native cardiac Ca^{2+} channels (Hess et al., 1984), activate through different pathways. We were able to show that silent and active traces had a tendency to cluster—a hallmark for the existence of gating modes—and that there appears to be at least two nonsilent modes as indicated by P_o histograms with logarithmic binning. Furthermore, nonparametric statistical tests show that P_o distribution for the two subunit combinations differ and that the P_o for β_{2a} is higher than for β_{1a}. This difference was also reflected in the frequency of traces with $P_o > 0.1$; fourfold higher for $\alpha_{1C}\beta_{2a}$ than for $\alpha_{1C}\beta_{1a}$. This increase in the likelihood of high P_o activity contributes significantly to the increase in coupling efficiency. However, the inherent variability in channel behavior prevented us from establishing whether channels underlying the expression of $\alpha_{1C}\beta_{2a}$ have a higher chance of entering the high P_o mode, or that stability of this mode is increased. This information is paramount to define the molecular mechanisms involved in the differential modulation of gating. On the other hand, log-binned P_o histograms revealed that of the two modes of gating, high P_o sweeps are of higher P_o with β_{2a} than β_{1a}, indicating that gating within this mode is also differentially regulated by the auxiliary subunit.

Opening and closing of the channel is fast and does not limit burst-durations

Consistent with the existence of at least two forms of channel activity, open-time histograms were better described by

several exponential components. We were able to partially isolate the component with the largest time constant by building open-time histograms from traces with $P_o > 0.1$ and fitting a single exponential distribution. Mean open-times measured in this manner were only slightly different for each subunit combinations. In contrast, MBDs were near twice as long for $\alpha_{1C}\beta_{2a}$ than for $\alpha_{1C}\beta_{1a}$ channels. If this increase reflects changes in the energy landscape of the final transition to the open state, differences in closing or opening rates should have been observed. Dwell-time histograms failed to reveal any changes in the rate of channel opening and the difference in mean open-times is insufficient to account for the increase in MBD. However, the combined effect of noise, filtering, and missed events was likely to have a significant impact on dwell-time histograms.

As a first approximation we applied the equations developed by McManus and co-workers (1987) to estimate true values for mean open-time and mean closed-time and found two possible solutions about an order-of-magnitude apart from each other. The simplest approach to determine which solutions correspond to the true mean dwell-time would have been to take recordings filtered at 5 or 10 kHz, but noise levels would make event detection virtually impossible. Algorithms capable of obtaining rate constants from noisy traces (Qin et al., 1996) were also of little help since they are model-dependent and unable to handle voltage-dependent channels displaying heterogeneous kinetics. Reasoning that the two possible solutions for the true mean dwell-times yield clearly different APDF, we compared them with the experimental data and found that neither of them was adequate. However, we did discover that the experimental APDF could be reproduced assuming opening and closing rates of 25,000 s^{-1} and 2500 s^{-1}, respectively. Simulated channels with these rates also reproduced quite well open-time and burst-duration histograms, indicating that opening and closing rates are an order-of-magnitude faster than previously thought. More importantly, the APDF for $\alpha_{1C}\beta_{1a}$ and $\alpha_{1C}\beta_{2a}$ are virtually identical, whereas changes in opening and closing rates sufficient to halve MBD result in clear differences in APDF. Together, these findings allow us to conclude that the exit rate to long-lived closed state is differentially modulated by the two β-subunits while opening and closing rates remain unchanged and consequently, structures controlling fast transitions in and out of the open state(s) are different from those limiting burst-durations.

Multiple gates controls channel opening

The idea that more that one structure can close voltage-dependent channels is not without precedent. Among the best-characterized examples are inactivation by the N-terminus of some K^+ channels (Hoshi et al., 1990), the III–IV domain linker of Na^+ channels (Patton et al., 1992), and the C-terminus of Ca^{2+} channel (de Leon et al., 1995). Structures in the pore of K^+ channels also have been shown to influence C-type inactivation (Lopez-Barneo et al., 1993). Here, the inactivation gate is unlikely to contribute to the observed differences in MBD, since voltage-dependent inactivation in $Ca_v1.2$ occurs in seconds (Neely et al., 1994). We cannot completely rule out yet that steady-state inactivation at the holding potential (−80 mV) may differ between $\alpha_{1C}\beta_{1a}$ and $\alpha_{1C}\beta_{2a}$, and contribute to changes in the number of nulls sweeps.

In addition to structures involved in long-lived non-conducting states, the pore region of the channel may also influence the lifetime of the open state. For example, K^+ channels with identical voltage sensors and divergent pore structures have mean open-time that differ by more than threefold (Kirsch et al., 1992). On the other hand, a construct of the *Shaker* K^+ channel that can be locked in the open conformation (Holmgren et al., 1997) can still display brief shut intervals at the single-channel level (Holmgren, personal communication). Interestingly, a detailed analysis of deactivation kinetic in *Shaker* channel suggests that this ''pore-gate'' give rise to conductance sublevels with a lifetime of few ms (Zheng et al., 2001). In light of these results it is plausible that in Ca^{2+} channels, brief shut intervals of ~40 μs may arise from the activity of a pore-gate. It is also reasonable to assume that this pore-gate involves structures in the outer vestibule of the channel and does not sense the presence of the β-subunit, as indicated by the virtual identity of the APDF for both subunit combinations.

Differential modulation of the MBD partially account for the increase in P_o

We have established that the MBD for $\alpha_{1C}\beta_{1a}$ is shorter than for $\alpha_{1C}\beta_{2a}$ but we have not discussed to what extent this phenomenon contributes to the difference in P_o we observed. Since opening and closing rates do not appear to be differentially modulated, the change in MBD reflects changes in the exit rate to long-lived closed states (k_{-1}). The impact that these changes will have on the channel P_o will depend mostly on the number of openings per burst. As the number of openings in a burst decreases, larger increases in k_{-1} will be needed to shorten the burst duration. As a consequence, the equilibrium will be shifted toward C_2 and the channel will wander among long-closed states several times before initiating a burst. This will produce a dramatic decrease in the P_o. In short, decreases in the MBD will be accompanied by large changes in P_o. In fact, the changes in P_o will increase asymptotically as the number of opening per bursts approaches to '1' (Fig. 11), suggesting that changes in k_{-1} may be responsible for all the changes we observed. For example, if $k_O = 1762$ s^{-1} and $k_C = 192$ s^{-1}, as we may derive from dwell-time histograms, a MBD of 8.40 ms is obtained with $k_{-1} = 2991$ s^{-1}. These values yield 1.6 openings per burst. Reducing k_{-1} to 998 s^{-1} augments the MBD to 15.1 ms and the number of openings per burst to

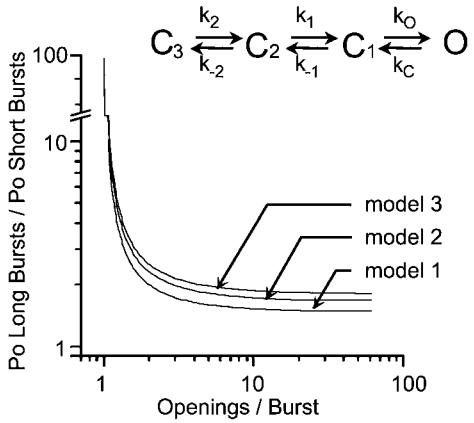

FIGURE 11 Calculated changes in P_o associated to a 1.8-fold decrease in MBD. The steady-state P_o for different four-states sequential models (*inset*) was calculated according to

$$P_O = \frac{1}{1 + k_C/k_O(1 + (k_{-1}/k_1)(1 + k_{-1}/k_2))},$$

and the changes in P_o expressed as the ratio between the calculated P_o for long bursts models ($MBD = 15.1$ ms) and the calculated P_o for short bursts ($MBD = 8.4$ ms),

$$\frac{P_O \text{ Long Bursts}}{P_O \text{ Short Bursts}} = \frac{1 + k_C/k_O(1 + k_{-1SMBD}/k_1(1 + k_{-2}/k_2))}{1 + k_C/k_O(1 + k_{-1LMBD}/k_1(1 + k_{-2}/k_2))},$$

k_{-1SMBD} and k_{-1LMBD}, were calculated using Eq. 8 when MBD was set to 8.4 ms and 15.1 ms, respectively. The plot shows the ratio P_oLong Bursts/P_oShort Bursts against the number of openings (*OPB*) in a short burst calculated from Colquhoun and Hawkes (1981), $OPB = 1 + k_O/k_{-1SMBD}$, for a series of k_O ranging from 1200 s^{-1} to 80,000 s^{-1} while $k_O/k_C = 10$. The latter is suggested by the experimental APDF. In addition, $1/(k_{-2} + k_1)$ was also kept constant (20 ms) to approximate the observed mean lifetime of long-lived closed states. With these considerations, when increasing k_O, OPB varied from 1.81 to 112.2 for long bursts and from 1.008 to 61.3 for short bursts. Three pairs of k_2 and k_{-2} values were examined. (*Model 1*) A three-states model obtained by virtually eliminating the sojourn in C_3 ($k_2 = 20{,}000$ s^{-1} and $k_{-2} = 0.1$ s^{-1}). In this case, when k_O was varied from 1200 s^{-1} to 80,000 s^{-1}, the P_o for long MBD changed from 0.24 to 0.38, whereas the ratio P_oLong Bursts/P_oShort Bursts changed from 89.5 to 1.48 as OPB increases. (*Model 2*) A four-states model in which the mean lifetime of C_3 and C_2 was set to 20 ms ($k_2 = 50$ s^{-1} and $k_{-2} = k_1 = 25$ s^{-1}). With this model, P_o for long MBD varies from 0.1 ($k_O = 1200$ s^{-1}) to 0.18 ($k_O = 80{,}000$ s^{-1}), whereas the P_oLong Bursts/P_oShort Bursts ratio approached 1.67 with large OPB. (*Model 3*). A four-states model in which the transition from C_2 to C_3 was decreased to obtain a P_o of 0.036 ($k_2 = 50$ s^{-1}, $k_{-2} = 44.8$ s^{-1}, and $k_1 = 5.2$ s^{-1}). In this case, the P_o for long MBD changed from 0.018 ($k_O = 1200$ s^{-1}) to 0.037 ($k_O = 80{,}000$ s^{-1}) and the ratio P_oLong Bursts/P_oShort Bursts from 98.5 to 1.81.

2.76. This change in MBD correlates with an increase in P_o that will vary from 2.4 to 3.2, depending on the number and duration of additional closed states. If this was the case, we may conclude that the differences in P_o stem only from changes in k_{-1}. On the other hand, we have shown that the APDF are only consistent with $k_O > 10{,}000$ s^{-1} and $k_O/k_C = 10$ and therefore, $\alpha_{1C}\beta_{1a}$ and $\alpha_{1C}\beta_{2a}$ channels open several times within a burst (>7). In this case, decreasing k_{-1} by near half will suffice to lengthen the MBD by ~1.8-fold that yields a comparable increase in P_o. However, the exact magnitude of the change in P_o will also vary with the model. For example, in a model with a silent mode and a high P_o mode with three states (*Model 1*), prolonging the MBD by decreasing k_{-1} will have a negligible impact on the frequency of bursts and the duration of gaps separating them. In this case, the P_o will increase only by ~1.5-fold. However, if the channel visits additional closed states frequently, the increase in P_o will be larger. In Model 2, for example, in which each time the channel reaches C_2 it has 50% chance of returning to C_3 ($k_{-2} = k_1 = 25$ s^{-1}), the minimum increase in P_o is 1.67-fold. When k_1 is reduced to 5.2 s^{-1} to reproduce the P_o values obtained from $\alpha_{1C}\beta_{2a}$ patches (0.036, Model 3), the channel returns to C_3 90% of the times it visits C_2. In this model, the minimum change in P_o is 1.8-fold. We can safely conclude then that the observed increase in the MBD contributes to a change in P_o between 1.5- and twofold. Therefore, the larger difference separating mean currents and macroscopic currents indicates additional changes such as the prevalence of the different gating modes.

Noceti and co-workers (1996) measured the number of charges per channel in $Ca_V2.3$ using two different methods and found an excess of charge movement not related to channel opening. This excess, observed when $Ca_V2.3$ was expressed by itself or together with β_{1a}, was greatly reduced with co-expression of β_{2a}. This observation led them to propose that there is reduction in the fraction of silent channels. The latter is indistinguishable from silent sweeps in single-channel patches and it would then appear that changes in coupling efficiency in $Ca_V2.3$ are mostly due to changes in the probability that channels enter a gating mode that never reaches the open state. Because $Ca_V2.3$ expressed alone displays activation kinetics similar to those observed when β_{2a} is co-expressed (Olcese et al., 1996), the changes in P_o should be mostly due to changes in the fraction of silent sweeps. On the other hand, there is a significant change in the activation time course when β_{2a} is co-expressed with $Ca_V1.2$ (α_{1C}; Neely et al., 1993) suggesting that additional changes in channel kinetics are involved. Together these observations are consistent with the view that changes in the MBD and the fraction of null sweeps together contribute to the changes in P_o we report here.

Modulation by other β-subunit

Xenopus oocytes express an endogenous β-subunit (β_{3xo}) that was shown to be required for the expression of functional Ca^{2+} channels (Tareilus et al., 1997). It was shown also that addition of cRNA encoding β_{3xo} changes the functional properties of a neuronal α_1 in the same manner as other β_3. It was then proposed that interaction with at least one β is necessary for expression, and that functional changes come about by interaction with an additional β. If each α_{1C} interacts with two β-subunits, shorter MBD may

arise from channels with an incomplete complement of β. This hypothesis is ruled out here by the observation that oocytes injected with α_{1C} cRNA by itself yield channels with MBD duration shorter than when co-injected with β_{1a} cRNA, and because addition of β_{3xo} cRNA yield channels with MBD longer than for $\alpha_{1C}\beta_{1a}$. Furthermore, the splice-variant β_{1b} of β_{1a} that comes from the same species as α_{1C} yields channels with similar MBD. These findings also show that the structures conferring the long MBD phenotype are shared between β_{2a} from rabbit and β_3 from *Xenopus*, whereas the ones for the short MBD phenotype are shared by β_{1a} and β_{1b}. We are currently investigating chimeras between different isoforms of the β-subunit to identify the structures associated with these phenotypes that will ultimately also help in identifying the molecular determinants regulating channel gating.

We thank C.J. Lingle, D. Naranjo and A. Zahradnikova for their insightful comments on the manuscript and S.J. Jones for kindly providing the source code of the software to perform convolution of the beta and Gaussian distributions.

This work was supported by grants from the National Institutes of Health (GM-53196) and the Fondo Nacional de Ciencia y Tecnología (1991016) to A.N.

REFERENCES

Bancroft, T. A., and C.-P. Han. 1981. Statistical Theory and Inference in Research. Marcek Dekker, New York.

Bichet, D., V. Cornet, S. Geib, E. Carlier, S. Volsen, T. Hoshi, Y. Mori, and M. De Waard. 2000. The I–II loop of the Ca^{2+} channel α_1 subunit contains an endoplasmic reticulum retention signal antagonized by the β-subunit. *Neuron.* 25:177–190.

Birnbaumer, L., N. Qin, R. Olcese, E. Tareilus, D. Platano, J. Costantin, and E. Stefani. 1998. Structures and functions of calcium channel β-subunits. *J. Bioenerg. Biomembr.* 30:357–375.

Brice, N. L., N. S. Berrow, V. Campbell, K. M. Page, K. Brickley, I. Tedder, and A. C. Dolphin. 1997. Importance of the differentβ-subunits in the membrane expression of the α_{1A} and α_2 calcium channel subunits: studies using a depolarization-sensitive α_{1A} antibody. *Eur. J. Neurosci.* 9:749–759.

Cavalie, A., D. Pelzer, and W. Trautwein. 1986. Fast and slow gating behavior of single calcium channel current in cardiac cells. *Pflugers Arch.* 406:241–248.

Chien, A. J., X. L. Zhao, R. E. Shirokov, T. S. Puri, C. F. Chang, D. Sun, E. Rios, and M. M. Hosey. 1995. Roles of a membrane-localized β-subunit in the formation and targeting of functional L-type Ca^{2+} channels. *J. Biol. Chem.* 270:30036–30044.

Colquhoun, D., and B. Sakmann. 1985. Fast events in single-channel currents activated by acetylcholine and its analogues at the frog muscle end-plate. *J. Physiol.* 369:501–557.

Colquhoun, D., and A. G. Hawkes. 1981. On the stochastic properties of single ion channels. *Proc. R. Soc. Lond. B Biol. Sci.* 211:205–235.

Costantin, J., F. Noceti, N. Qin, X. Wei, L. Birnbaumer, and E. Stefani. 1998. Facilitation by the β_{2a}-subunit of pore openings in cardiac Ca^{2+} channels. *J. Physiol.* 507:93–103.

de Leon, M., Y. Wang, L. Jones, E. Perez-Reyes, X. Wei, T. W. Soong, T. P. Snutch, and D. T. Yue. 1995. Essential Ca^{2+}-binding motif for Ca^{2+}-sensitive inactivation of L-type Ca^{2+} channels. *Science.* 270:1502–1506.

Fitzhugh, R. 1983. Statistical properties of the asymmetric random telegraph signal, with applications to single channel analysis. *Math. Biosci.* 64:75–89.

Hess, P., J. B. Lansman, and R. W. Tsien. 1984. Different modes of Ca^{2+} channel gating behaviour favored by dihydropyridine Ca^{2+} agonists and antagonists. *Nature.* 311:538–544.

Holmgren, M., P. L. Smith, and G. Yellen. 1997. Trapping of organic blockers by closing of voltage-dependent K^+ channels: evidence for a trap door mechanism of activation gating. *J. Gen. Physiol.* 109:527–535.

Horn, R., C. A. Vandenberg, and K. Lange. 1984. Statistical analysis of single sodium channels. Effects of *n*-bromoacetamide. *Biophys. J.* 45: 323–335.

Hoshi, T., W. N. Zagotta, and R. W. Aldrich. 1990. Biophysical and molecular mechanisms of *Shaker* potassium channel inactivation. *Science.* 250:533–538.

Kirsch, G. E., J. A. Drewe, M. Taglialatela, R. H. Joho, M. DeBiasi, H. A. Hartmann, and A. M. Brown. 1992. A single nonpolar residue in the deep pore of related K^+ channels acts as a K^+:Rb^+ conductance switch. *Biophys. J.* 62:136–143.

Lacerda, A. E., and A. M. Brown. 1989. Nonmodal gating of cardiac calcium channels as revealed by dihydropyridines. *J. Gen. Physiol.* 93: 1243–1273.

Lopez-Barneo, J., T. Hoshi, S. H. Heinemann, and R. Aldrich. 1993. Effects of external cations and mutations in the pore region on C-type inactivation of *Shaker* potassium channels. *Receptors Channels.* 1: 61–71.

Marks, T. N., and S. W. Jones. 1992. Calcium currents in the A7r5 smooth muscle-derived cell line. *J. Gen. Physiol.* 99:367–390.

McManus, O. B., A. L. Blatz, and K. L. Magleby. 1987. Sampling, log binning, fitting, and plotting durations of open and shut intervals from single channels and the effects of noise. *Pflugers Arch.* 410:530–553.

McManus, O. B., and K. L. Magleby. 1991. Accounting for the Ca^{2+}-dependent kinetics of single large- conductance Ca^{2+}-activated K^+ channels in rat skeletal muscle. *J. Physiol.* 443:739–777.

Naranjo, D., and P. Brehm. 1993. Modal shifts in acetylcholine receptor channel gating confer subunit-dependent desensitization. *Science.* 260:1811–1814.

Neely, A., R. Olcese, P. Baldelli, X. Wei, L. Birnbaumer, and E. Stefani. 1995. Dual activation of the cardiac Ca^{2+} channel α_{1C}-subunit and the modulation by the β-subunit. *Am. J. Physiol.* 268:C732–C740.

Neely, A., R. Olcese, X. Wei, L. Birnbaumer, and E. Stefani. 1994. Ca^{2+}-dependent inactivation of a cloned cardiac Ca^{2+} channel α_1 subunit (α_{1C}) expressed in *Xenopus* oocytes. *Biophys. J.* 66:1895–1903.

Neely, A., X. Wei, R. Olcese, L. Birnbaumer, and E. Stefani. 1993. Potentiation by the β-subunit of the ratio of the ionic current to the charge movement in the cardiac calcium channel. *Science.* 262:575–578.

Noceti, F., P. Baldelli, X. Wei, N. Qin, L. Toro, L. Birnbaumer, and E. Stefani. 1996. Effective gating charges per channel in voltage-dependent K^+ and Ca^{2+} channels. *J. Gen. Physiol.* 108:143–155.

Olcese, R., A. Neely, N. Qin, X. Wei, L. Birnbaumer, and E. Stefani. 1996. Coupling between charge movement and pore opening in vertebrate neuronal α_{1E} calcium channels. *J. Physiol.* 497:675–686.

Patton, D. E., J. W. West, W. A. Catterall, and A. L. Goldin. 1992. Amino acid residues required for fast Na^+-channel inactivation: charge neutralizations and deletions in the III–IV linker. *Proc. Natl. Acad. Sci. USA.* 89:10905–10909.

Pietrobon, D., B. Prodhom, and P. Hess. 1989. Interactions of protons with single open L-type calcium channels. pH dependence of proton-induced current fluctuations with Cs^+, K^+, and Na^+ as permeant ions. *J. Gen. Physiol.* 94:1–21.

Pragnell, M., J. Sakamoto, S. D. Jay, and K. P. Campbell. 1991. Cloning and tissue-specific expression of the brain calcium channel β-subunit. *FEBS Lett.* 291:253–258.

Prodhom, B., D. Pietrobon, and P. Hess. 1989. Interactions of protons with single open L-type calcium channels. Location of protonation site and

dependence of proton- induced current fluctuations on concentration and species of permeant ion. *J. Gen. Physiol.* 94:23–42.

Qin, F., A. Auerbach, and F. Sachs. 1996. Estimating single-channel kinetic parameters from idealized patch-clamp data containing missed events. *Biophys. J.* 70:264–280.

Ruth, P., A. Rohrkasten, M. Biel, E. Bosse, S. Regulla, H. E. Meyer, V. Flockerzi, and F. Hofmann. 1989. Primary structure of the β-subunit of the DHP-sensitive calcium channel from skeletal muscle. *Science.* 245:1115–1118.

Sanford, J., J. Codina, and L. Birnbaumer. 1991. γ-subunit of G-proteins, but not their α- or β-subunits, are polyisoprenylated. *J. Biol. Chem.* 266:9570–9579.

Sigworth, F. J., and S. M. Sine. 1987. Data transformations for improved display and fitting of single-channel dwell-time histograms. *Biophys. J.* 52:1047–1054.

Singer, D., M. Biel, I. Lotan, V. Flockerzi, F. Hofmann, and N. Dascal. 1991. The roles of the subunits in the function of the calcium channel. *Science.* 253:1553–1557.

Stea, A., S. J. Dubel, M. Pragnell, J. P. Leonard, K. P. Campbell, and T. P. Snutch. 1993. A β-subunit normalizes the electrophysiological properties of a cloned N-type Ca^{2+} channel α_1 subunit. *Neuropharmacology.* 32:1103–1116.

Taglialatela, M., L. Toro, and E. Stefani. 1992. Novel voltage clamp to record small, fast currents from ion channels expressed in *Xenopus* oocytes. *Biophys. J.* 61:78–82.

Tareilus, E., M. Roux, N. Qin, R. Olcese, J. M. Zhou, E. Stefani, and L. Birnbaumer. 1997. A *Xenopus* oocyte β-subunit: Evidence for a role in the assembly/expression of voltage-gated calcium channels that is separate from its role as a regulatory subunit. *Proc. Natl. Acad. Sci. USA.* 94:1703–1708.

Van Dongen, A. M. 1996. A new algorithm for idealizing single ion channel data containing multiple unknown conductance levels. *Biophys. J.* 70:1303–1315.

Villarroel, A., O. Alvarez, A. Oberhauser, and R. Latorre. 1988. Probing a Ca^{2+}-activated K^+ channel with quaternary ammonium ions. *Pflugers Arch.* 413:118–126.

Wakamori, M., G. Mikala, and Y. Mori. 1999. Auxiliary subunits operate as a molecular switch in determining gating behaviour of the unitary N-type Ca^{2+} channel current in *Xenopus* oocytes. *J. Physiol.* 517:659–672.

Wakamori, M., G. Mikala, A. Schwartz, and A. Yatani. 1993. Single-channel analysis of a cloned human heart L-type Ca^{2+} channel α_1 subunit and the effects of a cardiac β-subunit. *Biochem. Biophys. Res. Commun.* 196:1170–1176.

Wei, X., A. Neely, R. Olcese, W. Lang, E. Stefani, and L. Birnbaumer. 1996. Increase in Ca^{2+} channel expression by deletions at the amino terminus of the cardiac α_{1C}-subunit. *Receptors Channels.* 4:205–215.

Wei, X. Y., E. Perez Reyes, A. E. Lacerda, G. Schuster, A. M. Brown, and L. Birnbaumer. 1991. Heterologous regulation of the cardiac Ca^{2+} channel α_1 subunit by skeletal muscle β- and γ- subunits. Implications for the structure of cardiac L-type Ca^{2+} channels. *J. Biol. Chem.* 266: 21943–21947.

Williams, M. E., D. H. Feldman, A. F. McCue, R. Brenner, G. Velicelebi, S. B. Ellis, and M. M. Harpold. 1992. Structure and functional expression of α_1-, α_2-, and β-subunits of a novel human neuronal calcium channel subtype. *Neuron.* 8:71–84.

Yellen, G. 1984. Ionic permeation and blockade in Ca^{2+}-activated K^+ channels of bovine chromaffin cells. *J. Gen. Physiol.* 84:157–186.

Zheng, J., L. Vankataramanan, and F. J. Sigworth. 2001. Hidden Markov model analysis of intermediate gating steps associated with the pore gate of *Shaker* potassium channels. *J. Gen. Physiol.* 118:547–562.